Inelastic scattering of electron and light ion beams in organic polymers

Pablo de Vera,[1,a)] Isabel Abril,[1] and Rafael Garcia-Molina[2]
[1]*Departament de Física Aplicada, Universitat d'Alacant, E-03080 Alacant, Spain*
[2]*Departamento de Física - Centro de Investigación en Óptica y Nanofísica, Universidad de Murcia, E-30100 Murcia, Spain*

(Received 18 January 2011; accepted 11 March 2011; published online 3 May 2011)

We have calculated the inelastic mean free path, stopping power, and energy-loss straggling of swift electron, proton, and α-particle beams in a broad incident energy range in four organic polymers: poly(methyl methacrylate) (PMMA), Kapton, polyacetylene (PA), and poly(2-vinylpyridine) (P2VP). These calculations have been done through a suitable description of their optical properties and its extension into the whole momentum and energy transfer excitation spectrum. For electrons, we take into account the exchange effect between the projectile and the target electrons, while the charge-state fractions have been considered for ions. Our results are compared with other models and with the available experimental data. An excellent agreement with experimental data is obtained in the case of proton and α-particle beams in Kapton and a reasonably good agreement has been achieved for electron beams in PMMA, Kapton, and PA. We have parameterized by means of simple analytical expressions our results for electron beams interacting with these four polymers, which can be easily implemented in Monte Carlo calculations. © *2011 American Institute of Physics*. [doi:10.1063/1.3581120]

I. INTRODUCTION

Polymers are materials of special importance due to their extensive applications in diverse areas of physics, chemistry, materials science, and nanoscience. For example, PMMA has been widely used as a positive electron-beam resist in electron-beam lithography,[1,2] and it is important to know the spatial distribution of the energy deposited on it to improve the resolution of the patterns made by this procedure. Also this technique can be combined with ion implantation, Rutherford backscattering, and electronic microscopy to obtain nanostructures,[3] waveguides,[4] or modify the electrical properties of materials.[5] Moreover, PMMA is commonly used as a water phantom in dosimetry measurements for radiotherapy.[6] Kapton is an excellent insulator, very resistant to radiation effects especially at high temperature; therefore, it is used invariably as a thermal blanket in the outer surface of satellite structures. In this type of environments, radiation can build up a positive or negative charge in Kapton pieces, so it is crucial to know accurately these effects to guarantee the survival of the satellite.[7] In addition, polymers have been widely used in the human body due to their singular properties, such as low weight, facility to shape, or chemical inertness in biological environments. The great variety of different kinds of polymers allows to select the best suitable material for a given biomedical application.[8]

Irradiation with energetic ion beams offers a possibility to modify both the structural and the functional properties of polymers to tailor them as useful materials for different applications.[9] These modifications are possible due to the high energy delivered by the ion beam into the target, reaching up to hundreds of electron volts per nanometer. In addition, polymers are much more sensitive to radiation than inorganic targets, resulting in scission, cross-linking, and graphitization.[10] This damage can be exploited for improving properties of thin films,[11] creating graphitic nanostructures[3] or organic transistors.[12] Therefore ion beam modification of polymers is a well established technique to change their tribological properties (hardness, Young modulus, friction),[13,14] as well as wetability and/or cell adhesion.[8]

Although stopping power data of polymers for charged particles are highly demanded, it is not possible to obtain experimental data for all the combinations of projectiles and polymers in an extended range of incident energies. Thus an advantageous alternative is to dispose of a reliable theory capable of calculating the electronic energy-loss of the projectile in a given target.

For projectiles in the high-energy range, Bethe theory[15] can be used for the calculation of the stopping power. However, this theory requires a material-dependent parameter, the mean excitation energy I, and additional theoretical calculations for shell corrections. At intermediate energies, stopping power calculations for ions are complex because of changing mechanisms of ion-electron interactions. In addition, compound targets, such as polymers, manifest aggregation effects due to both chemical bonding and physical state. A first approximation in the investigation of these aggregation effects in the stopping power of compound targets was proposed by Bragg and Kleeman,[16] assuming a weighted additivity of the stopping cross-sections of its elemental constituents. However, this assumption, called Bragg's (or additivity) rule, is not totally suitable because it does not take into account the effect of chemical bonds and physical state. Deviations of measured stopping powers from the additivity rule in compounds have been extensively reported.[17,18]

In this paper we use the dielectric formalism[19] together with the Mermin energy-loss function-generalized oscillator strength (MELF-GOS) method[20,21] to calculate the energy loss of electron, proton, and α-particle beams through

a)Electronic mail: pablo.vera@ua.es.

electronic excitations in four organic polymers for a wide interval of projectile energies, including the maximum stopping power region. The advantage of this treatment lies in the fact that it is not necessary to know the mean excitation energy (in fact, it is an output of our calculations), and it includes, in a self-consistent way, the shell corrections and aggregation effects of the target. This procedure has been successfully applied to find the energy-loss of light ions in monoatomic,[22,23] as well as in compound targets, with complex excitation spectra,[21,24–26] showing a satisfactory agreement with the experimental data.

In what follows, we present the essentials of the theoretical formalism used, which is applied to calculate the inelastic mean free path, stopping power and energy-loss straggling for four widely used solid organic polymers: poly(methyl methacrylate) (PMMA), Kapton, polyacetylene (PA), and poly(2-vinylpyridine) (P2VP), for the case of electron, proton, and α-particle beams. In Table I, we present the main properties of these polymers, such as their formula, atomic number Z_2, and atomic mass A_2 (that is, the sum of the atomic and mass numbers of the elemental constituents of the compound), mass density ρ, molecular density $\mathcal{N}$, and number of valence electrons per molecule N_V. Our calculations are compared with available experimental data and with other theoretical results, finding a good agreement with experiments, even better than other models. For electrons, we analyze the effect of electron exchange. We also obtain the mean excitation energy of these polymers and compare them with values based in Bragg's rule or in stopping power measurements.

II. THEORETICAL BACKGROUND

A. Dielectric formalism

Due to the stochastic nature of the electronic excitations induced by the passage of a swift projectile through a medium, its energy-loss distribution, ΔE, per unit path length, Δx, is characterized by the moments $\langle \Delta E^n \rangle / \Delta x$.

The zero moment ($n=0$) corresponds to the inverse inelastic mean free path (λ^{-1}), which is related to the cross-section σ for an inelastic event by $\lambda^{-1} = \mathcal{N}\sigma$, where $\mathcal{N}$ is the target density of scattering centers.

The first moment ($n=1$) is the mean energy loss per unit path length, which is called stopping power or stopping force, S. The stochastic fluctuations in the energy lost by the projectile are accounted for by the second moment ($n=2$), which is the so called energy-loss straggling, Ω^2, being related to the variance of the energy loss per unit path length.

Within the linear dielectric formalism,[19] the moments of the energy-loss distribution of a projectile, moving with velocity v through a target characterized by a dielectric function ε, is given by:

$$\frac{\langle \Delta E^n \rangle}{\Delta x} = \frac{2e^2}{\pi v^2} \int_0^{\omega_{max}} d\omega (\hbar\omega)^n \int_{k_-}^{k_+} \frac{dk}{\hbar k} F(k) \mathrm{Im}\left[\frac{-1}{\varepsilon(k,\omega)}\right], \quad (1)$$

where e is the elemental charge, $\hbar k$ and $\hbar\omega$ are, respectively, the momentum and energy transfer to the target in an inelastic event, and $\mathrm{Im}[-1/\varepsilon(k,\omega)]$ is called the energy-loss function (ELF) of the material, which contains all the information about the electronic excitations of the target. $F(k)$ is the form factor, related with the projectile charge density, through $F(k) = |Z_1 - f(k)|^2$, where Z_1 is the projectile atomic number and $f(k)$ is the Fourier transform of its electronic density.

The integration limits in the momentum transfer in Eq. (1), based in conservation laws, are $k_\pm = Mv/\hbar \pm \sqrt{(Mv/\hbar)^2 - 2M\omega/\hbar}$. For heavy projectiles, with mass M much larger than the electron mass ($M \gg m_e$), Eq. (1) admits the following simplifications: $k_- = \omega/v$, $k_+ \to \infty$ and $\omega_{max} \to \infty$.

At low and intermediate velocities, the projectile continually captures and loses electrons; therefore these charge-exchange processes must be considered. We include these processes considering the equilibrium charge state fraction of the projectile, ϕ_q. Therefore, we rewrite the form factor $F(k)$ as:

$$F(k) = \sum_{q=0}^{Z_1} \phi_q |Z_1 - f_q(k)|^2, \quad (2)$$

where q is the charge state of the projectile, and $f_q(k)$ is the Fourier transform of the projectile electronic density of charge q, which is modeled by the Brandt–Kitagawa theory.[31] To obtain ϕ_q, which depends on the projectile velocity and the target nature, we use the values obtained by the CasP code,[32] where ϕ_q for compound targets has been obtained applying Bragg's rule to each element of the target.

When the projectile is an electron, $F(k) = 1$. However, in this case, it is necessary to take into account the indistinguishability between the incident (or primary) electron and the hit target electron. We consider that primary electrons are always the most energetic after the collision, and therefore $\omega_{max} = m_e v^2/4$ in Eq. (1).

B. MELF-GOS method

To obtain from Eq. (1) the projectile energy-loss distribution, it is necessary to know the energy-loss function of the target in the whole Bethe surface, that is, for all the

TABLE I. Properties of the polymers studied in this work.

Material	Formula	Z_2	A_2	ρ (g/cm^3)	$\mathcal{N}$ (molec/Å^3)	N_V (from Ref. 30)
PMMA	$(C_5H_8O_2)_n$	54	100.116	1.188 (Ref. 27)	7.14×10^{-3}	40
Kapton	$(C_{22}H_{10}N_2O_5)_n$	196	385.325	1.417 (Ref. 28)	2.23×10^{-3}	138
PA	$(CH)_n$	7	13.0189	1.36 (Ref. 29)	6.29×10^{-2}	5
P2VP	$(C_7H_7N)_n$	56	105.137	1.153 (Ref. 27)	1.45×10^{-4}	40

momenta, $\hbar k$, and energies, $\hbar\omega$, transferred to the target. We use the MELF-GOS method[20,21] to describe the electronic excitation spectrum of the target. In this method, we treat separately the outer electronic excitations (more sensitive to aggregation effects) and the inner-shell electronic excitations (which maintain their atomic nature), namely

$$\begin{aligned}\mathrm{Im}\left[\frac{-1}{\varepsilon(k,\omega)}\right] &= \mathrm{Im}\left[\frac{-1}{\varepsilon(k,\omega)}\right]_{\mathrm{outer}} + \mathrm{Im}\left[\frac{-1}{\varepsilon(k,\omega)}\right]_{\mathrm{inner}} \\ &= \underbrace{\sum_i A_i \mathrm{Im}\left[\frac{-1}{\varepsilon_{\mathrm{M}}(\omega_i,\gamma_i;k,\omega)}\right]\Theta(\omega-\omega_{\mathrm{th},i})}_{\text{outer electrons}} \\ &+ \underbrace{\frac{2\pi^2\mathcal{N}}{\omega}\sum_j \alpha_j \sum_{n\ell}\frac{\mathrm{d}f_{n\ell}^{(j)}(k,\omega)}{\mathrm{d}\omega}\Theta(\omega-\omega_{\mathrm{ioniz},n\ell}^{(j)})}_{\text{inner-shell electrons}}.\end{aligned} \tag{3}$$

The first term in the right hand side of this equation describes the outer electronic excitations, that is, individual and collective ones. The excitations at $k = 0$ are fitted to the optical experimental energy-loss function (OELF) by means of a weighted sum of Mermin-type ELFs, where ε_{M} is the Mermin dielectric function.[33] The fitting parameters ω_i and γ_i correspond to the position and width, respectively, of the ith Mermin-type ELF, while the coefficients A_i are their weights; $\hbar\omega_{\mathrm{th}}$ is a threshold energy. To obtain the Bethe surface, the extension of the ELF at $k \neq 0$ is automatically given through the analytical dependence of the Mermin-type ELF. Therefore it is not necessary to propose a dispersion relation, as it is done in other models.[34–37] We have checked the ELF at $k \neq 0$ given by the MELF-GOS method with available experimental data, obtaining a good agreement.[23,38,39]

The second term in the right hand side of Eq. (3) corresponds to the inner-shell electronic excitations, which have large binding energies and preserve their atomic nature; therefore they are suitably modeled in terms of the generalized oscillator strengths (GOS) in the hydrogenic approach.[40] $\mathrm{d}f_{n\ell}^{(j)}(k,\omega)/\mathrm{d}\omega$ is the GOS of the (n,ℓ)-subshell, $\hbar\omega_{\mathrm{ioniz},n\ell}$ is the ionization energy of the (n,ℓ)-subshell and α_j is the stoichiometry of the jth elemental constituent of the compound.

C. Sources of optical data

In Fig. 1 we represent by symbols the experimental ELF in the optical limit, ELF($k = 0$, ω), of PMMA,[41] Kapton,[42] PA,[43] and P2VP (Ref. 44); the MELF-GOS fittings for each material are shown by solid lines. For Kapton [Fig. 1(b)], there are in the literature two different sets of experimental ELFs, one obtained by reflectance measurements from 0.5 to 70 eV by Arakawa *et al.*[42] and the other by reflection electron energy-loss spectroscopy (REELS) from 0 to 40 eV by Mondio *et al.*[45] We have decided to use the former optical data because the latter use these data to determine the superficial contribution of their measurements, having to do many corrections to their experiment and because optical data from Ref. 42 match better with high transferred energy data from Henke *et al.*[46]

At high transferred energies, where there are no experimental data of the ELF, we use the experimental results of the refractive index, n, and the extinction coefficient, κ, from Henke *et al.*,[46] which allow to obtain the ELF because $\varepsilon = (n + i\kappa)^2$, applying Bragg's rule to the ELF of the elemental constituents of each polymer. We treated the K-shell of C, N, and O as inner shells with ionization energies of 284.2, 409.9, and 543.1 eV, respectively.[47] The outer electronic excitations are fitted using the parameters appearing in Table II.

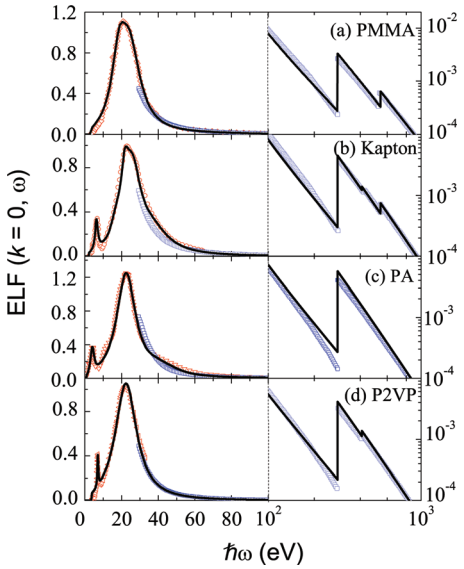

FIG. 1. (Color online) Energy loss function, ELF, in the optical limit ($k = 0$) of: (a) PMMA, (b) Kapton, (c) PA, and (d) P2VP as a function of the transferred energy, $\hbar\omega$. Solid curves were obtained through the MELF-GOS method (as described in the text), whereas experimental data for $\hbar\omega < 100$ eV were taken from different sources: (a) ◇ (Ref. 41), (b) ◯ (Ref. 42), (c) ▽ (Ref. 43), and (d) ◁ (Ref. 44). The symbols (□) correspond to the ELF values at high transferred energies obtained from x-ray scattering factors (Ref. 46).

The energy-loss function of a target constructed by the MELF-GOS method must verify the f-sum rule and the Kramers-Kronig (or perfect screening) sum rule.[30] The first one is satisfied better than 1% for all polymers, and the second one is also satisfied within an error of a few percent.

TABLE II. Parameters used to fit the outer electronic excitations through Eq. (3).

Material	i	$\hbar\omega_i$ (eV)	$\hbar\gamma_i$ (eV)	A_i
PMMA	1	19.13	9.03	2.59×10^{-1}
$\hbar\omega_{th} = 2.99$ eV	2	25.36	14.34	4.46×10^{-1}
	3	70.75	48.98	4.44×10^{-3}
Kapton	1	6.45	1.90	8.01×10^{-2}
$\hbar\omega_{th} = 2.32$ eV	2	17.14	6.26	5.04×10^{-2}
	3	20.91	5.31	1.01×10^{-1}
	4	26.53	11.16	2.84×10^{-1}
	5	38.10	23.13	1.22×10^{-1}
PA	1	4.22	2.31	1.65×10^{-1}
$\hbar\omega_{th} = 0.95$ eV	2	23.40	12.83	6.63×10^{-1}
	3	39.46	13.61	1.90×10^{-2}
	4	46.26	19.05	2.42×10^{-2}
P2VP	1	7.11	0.49	2.33×10^{-2}
$\hbar\omega_{th} = 3.59$ eV	2	23.50	14.33	6.27×10^{-1}
	3	54.42	40.82	7.5×10^{-3}

TABLE III. Mean excitation energy I (eV) of the four polymers, obtained by several methods.

Material	Present work	ICRU (Bragg's rule)	Akkerman and Akkerman (Ref. 37)	Tan *et al*. (Ref. 51)	Porter (Ref. 52)
PMMA	70.3	74.0 ±1.5 (Ref. 49)	68.5	68.37	—
Kapton	82.4	79.6 (Ref. 49)	—	76.30	80.64
PA	73.7	65.9 (Ref. 50)	67.5	63.80	—
P2VP	70.0	67.8 (Ref. 50)	65.2	65.74	—

III. RESULTS AND DISCUSSION

One expression widely used to calculate the stopping power for fast charged particles is the Bethe formula,[15,48] where the main parameter is the mean excitation energy I, which is a characteristic of the target. One of the outputs of the MELF-GOS method is the I value, obtained through the following expression

$$\ln I = \frac{\int_0^\infty d\omega' \omega' \ln \omega' \mathrm{Im}[-1/\varepsilon(k=0,\omega')]}{\int_0^\infty d\omega' \omega' \mathrm{Im}[-1/\varepsilon(k=0,\omega')]}. \quad (4)$$

In Table III we show the calculated I values from the MELF-GOS method corresponding to the four polymers discussed in this work: PMMA, Kapton, PA, and P2VP. To check departures from the additivity rule, we compare our results with the mean excitation energy I_B obtained by simple application of Bragg's rule,[50] namely

$$\ln I_B = \frac{\sum_j \nu_j (Z_j/A_j) \ln I_j}{\sum_j \nu_j Z_j/A_j}, \quad (5)$$

where ν_j, Z_j, A_j, and I_j, represent, respectively, the fraction by weight, the atomic number, the mass number, and the mean excitation energy of the jth elemental component of the compound material. Results obtained by Akkerman and Akkerman[37] and by Tan *et al*.[51] from Eq. (4) are also included in Table III. A value of I extracted from stopping power measurements for protons and alpha particles in Kapton in the MeV energy range is also presented,[52] although in this case, the dispersion of the experimental data makes it difficult to obtain accurate values of the mean excitation energy I. Differences between the I values obtained by the MELF-GOS method with respect to the I_B values are attributed to aggregation effects of the compound, which present the largest deviations in low-Z materials because a large fraction of the total number of electrons participates in the bonding.

A. Electron beams

We present in Figs. 2 and 3 our calculations of the inelastic mean free path, λ, and the stopping power, S, of electrons interacting with (a) PMMA, (b) Kapton, (c) PA, and (d) P2VP targets. We restrict our results to nonrelativistic electrons with energies ranging from 10 eV to 10 keV. These calculations take into account the exchange effect between the incident electron and the target electrons through the Born–Ochkur approximation,[53] which consists in multiplying the integrand in Eq. (1) by the exchange factor $f_{ex} = 1 - (k/v)^2 + (k/v)^4$. This approximation must be considered a lower limit in the stopping power (and an upper limit in the mean free path), because the Ochkur exchange correction is based on the assumption of single-electron excitations; however, the Mermin-type ELF does not allow to separate individual and collective electron excitations.

To evaluate the influence of the exchange effect, we also show in Figs. 2 and 3 the inelastic mean free path and the stopping power when calculated with and without this effect (solid black and gray lines, respectively). As can be seen in Fig. 2, the influence of the exchange effect on the mean free path λ is in the valley region ($E \approx 100$ eV) $< 10\%$ in general. The difference becomes less important ($\sim 5\%$) at 200 eV and even less at higher energies. For the stopping power S, the exchange effect gives also a difference $< 10\%$ at the maximum ($E \approx 100$ eV), as it is shown in Fig. 3. This difference also becomes smaller at high energies, but more slowly, being $\sim 8\%$ at 200 eV and $< 5\%$ above 400 eV.

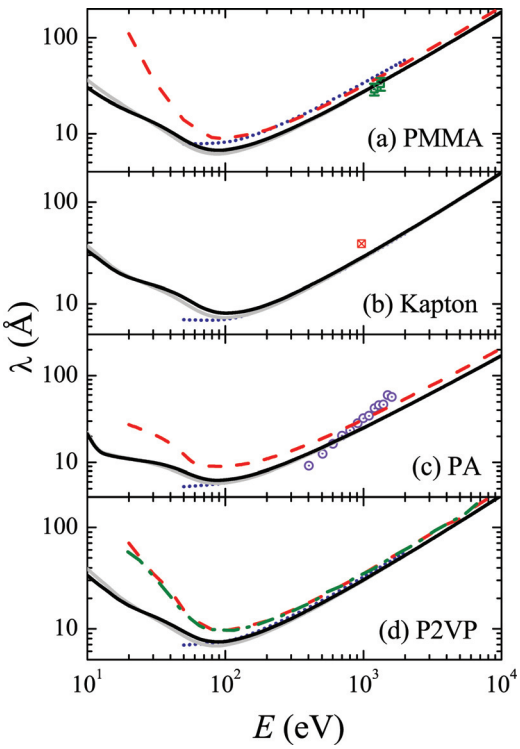

FIG. 2. (Color online) Inelastic mean free path of electrons in: (a) PMMA, (b) Kapton, (c) PA, and (d) P2VP, as a function of incident kinetic energy. Solid black and gray lines are the results from the MELF-GOS method in this work with and without the Born–Ochkur exchange correction (Ref. 53), respectively. Dotted lines are the results from the TPP model without exchange correction (Ref. 30). Dashes lines in (a), (c), and (d) are the results from Akkerman and Akkerman (Ref. 37) with Ashley's exchange. Dash-dotted line in (d) is the result from Tan *et al* (Ref. 51). with Born–Ochkur exchange. Available experimental data are presented by symbols: ⊡ PMMA (Ref. 54), ⊠ Kapton (Ref. 55), and ⊙ PA (Ref. 58).

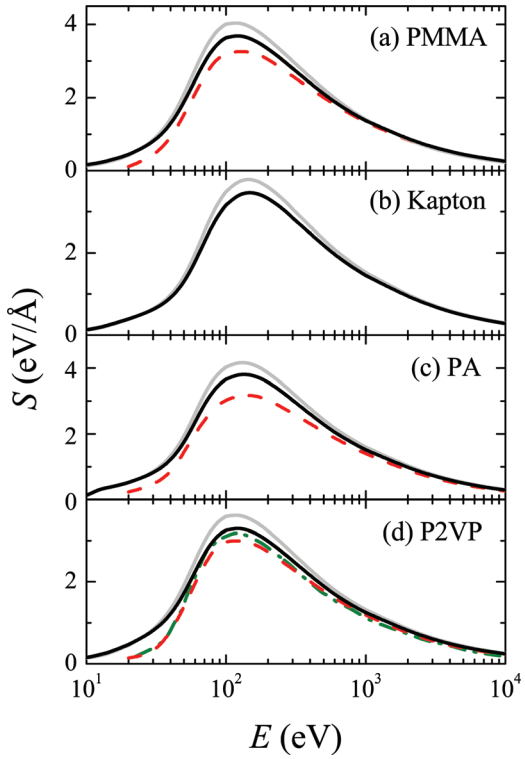

FIG. 3. (Color online) Stopping power of (a) PMMA, (b) Kapton, (c) PA, and (d) P2VP for an electron beam, as a function of incident kinetic energy. Solid black and gray lines correspond to the results obtained from the MELF-GOS method in this work with and without the Born–Ochkur exchange correction (Ref. 53), respectively. Dashed lines in (a), (c), and (d) are the results from Akkerman and Akkerman (Ref. 53) with Ashley's exchange factor. Dash-dotted line in (d) is the result from Tan *et al*. (Ref. 53) with Born–Ochkur exchange.

Our results for λ can be compared with experimental data in the case of electrons interacting with PMMA, Kapton, and PA. It is worth noting how our calculations are in excellent agreement with the measurements in PMMA,[54] Fig. 2(a), better than the results of the other models shown in the figure. For Kapton, there is only one measurement at 967 eV by Cadman *et al*.,[55] which lies ~30% above all the calculations. The inelastic mean free path in the case of PA has been investigated in Refs. 56–58; the experimental data shown in Fig. 2(d) were reported in the more recent publication.[58] The slope of these data cannot be reproduced by any model. Nevertheless, the same group reports very different experimental values in its previous publications.[56,57]

In Fig. 2 we also compare our results, obtained by the MELF-GOS method, with calculations developed by Tanuma *et al*.[30] (dotted lines), Akkerman and Akkerman[37] (dashed lines), and Tan *et al*.[51] (dash-dotted line), based on the dielectric response theory but using different approaches to describe the ELF of the target. Our calculations agree well (except for PMMA) with the TPP predictions[30] at high energy ($\geq$200 eV), but differences appear at the valley region where the TPP curves go below our results. Concerning the rest of models, there are differences in λ of ~30% at the valley region and ~15% at energies above 1 keV.

In the case of the stopping power S, Fig. 3, our calculations are also compared with the ones by Akkerman and Akkerman[37] and Tan *et al*.[51] Now, all the models agree at high energies, but the differences around the maximum are $\geq$10%. Such differences in λ and S are due to the different approaches taken to extend the optical ELF($k = 0$, ω) into $k \neq 0$. Although both groups[37,51] work with Drude dielectric functions to fit the experimental OELF, the former[37] uses a weighted sum of Drude functions, and the latter[51] uses a single Drude function. Nonetheless, both extend the ELF at $k \neq 0$ by means of a simple quadratic dispersion relation. In fact, it can be seen how these calculations[37,51] resemble each other, due to their similar approaches. In the case of TPP model,[30] the Penn ELF is used, but also a quadratic dispersion relation is introduced. It is not the case of the MELF-GOS method, where the dependence of the ELF with k is naturally included through the functional form of the Mermin dielectric functions $\varepsilon_M(k, \omega)$ and the GOS. In this sense, the extension of the ELF into $k \neq 0$ is properly described by our model, so we expect more reliable values of the stopping magnitudes. In fact, it has been shown, in the case of several targets,[23,38,39] how the MELF-GOS method describes the electronic excitation spectrum in the (k-ω) space better than Drude's and Penn's approaches.

To make easier and faster the implementation of our calculations in a Monte Carlo simulation code, in what follows we provide analytical expressions (with the corresponding parameters) that adjust remarkably well to our results. For λ (in Å) we have used the modified form of the Bethe equation for the incident energy dependence of the inelastic electron scattering in matter[30]

$$\lambda(E) = \frac{E}{E_P^2[\beta \ln(\Gamma E) - C/E + D/E^2]}, \qquad (6)$$

where E is the electron energy (in eV), $E_P = 28.8\sqrt{N_V \rho / A_2}$ (in eV) is the nominal bulk plasmon energy, and β, Γ, C, and D are fitting parameters. N_V is the number of valence electrons per molecule, which has been taken from Ref. 30; ρ is the density of the polymer in g/cm^3 and A_2 is its mass number (see Table I). An excellent fitting to our results has been achieved with Eq. (6) in the range 10 eV to 10 keV using the parameters shown in Table IV. It is worth to note that although the exchange correction is overestimated in the calculations (because Born–Ochkur correction is only valid for individual excitations and Mermin ELFs do not allow to distinguish them from the collective excitations), we expect the corrected results to have an error of only a few percent because individual excitations are dominant in the range of energy considered in this work.

TABLE IV. Parameters used to apply Eq. (6) to the four polymers discussed in this work.

Material	β (eV^{-1} Å^{-1})	Γ (eV^{-1})	C (Å^{-1})	D (eV Å^{-1})	E_P (eV)
PMMA	0.0180	0.206	2.006	32.094	19.842
Kapton	0.0162	0.186	2.278	49.789	20.597
PA	0.0177	0.207	2.097	27.739	20.814
P2VP	0.0175	0.200	1.913	31.146	19.075

Kumagai *et al.*[59] have developed an expression with adjustable parameters for the stopping power S of electrons that, in eV/Å, reads

$$S(E) = \frac{784.6 Z_2 \rho}{E A_2} \sum_{i=1}^{m} \frac{a_i}{n_i} \ln\left[1 + \left(\frac{E}{b_i}\right)^{n_i}\right], \qquad (7)$$

where E is the electron energy in eV, ρ is the target density in g/cm^3 and a_i, b_i, and n_i are fitting parameters. By using only one term in the sum, we have achieved an excellent fitting to our calculated data in the range 50–1000 eV, so we can fit our results, for $E \leq 1$ keV, with

$$S(E) = \frac{784.6 Z_2 \rho}{E A_2} \frac{a_1}{n_1} \ln\left[1 + \left(\frac{E}{b_1}\right)^{n_1}\right], \qquad (8)$$

being a_1, b_1, and n_1 the parameters given in Table V.

For higher energies, it is justified the use of Bethe formula for these polymers because the excitation thresholds of all the inner-shells involved are overtaken. Therefore, for $E > 1$ keV, the next equation should be used

$$S(E) = \frac{784.6 Z_2 \rho}{E A_2} \ln\left(\frac{1.166E}{I}\right), \qquad (9)$$

where the value of I is that calculated by the MELF-GOS method (see Table III).

B. Light ion beams

The MELF-GOS method results for the electronic stopping power of proton and α-particle beams in the polymers PMMA, Kapton, PA, and P2PV are depicted in Fig. 4 by solid lines. The calculated data cover a wide range of incident energies, including the maximum stopping power region. We neglect the contribution of nuclear stopping power because it is very small in the energy range considered in this work, especially for low-Z targets.[60] We have checked that the nuclear stopping contribution to the total stopping power is of a few percent below 10 keV/u (< 2 % for protons and < 4 % for alphas), where our calculations cannot be applied because these energies are too low to use the Born approximation. At 25 keV/u, the nuclear stopping is < 1 % for protons and < 2 % for alphas, and always < 1 % above 50 keV/u for both projectiles.

For these calculations, it is important a proper extension of the optical ELF in the whole Bethe surface taking into account the solid-state effects, but also the electron exchange processes between the projectile and the target should be considered. This charge state effect is included through Eq. (2). As it has been explained in Sec. II, we take the equilibrium

TABLE V. Parameters used in Eq. (8) to fit our calculated S for the four polymers studied in this work.

Material	a_1	b_1 (eV)	n_1
PMMA	0.877	44.317	5.031
Kapton	0.892	54.333	4.332
PA	0.993	48.474	4.477
P2VP	0.791	44.577	4.752

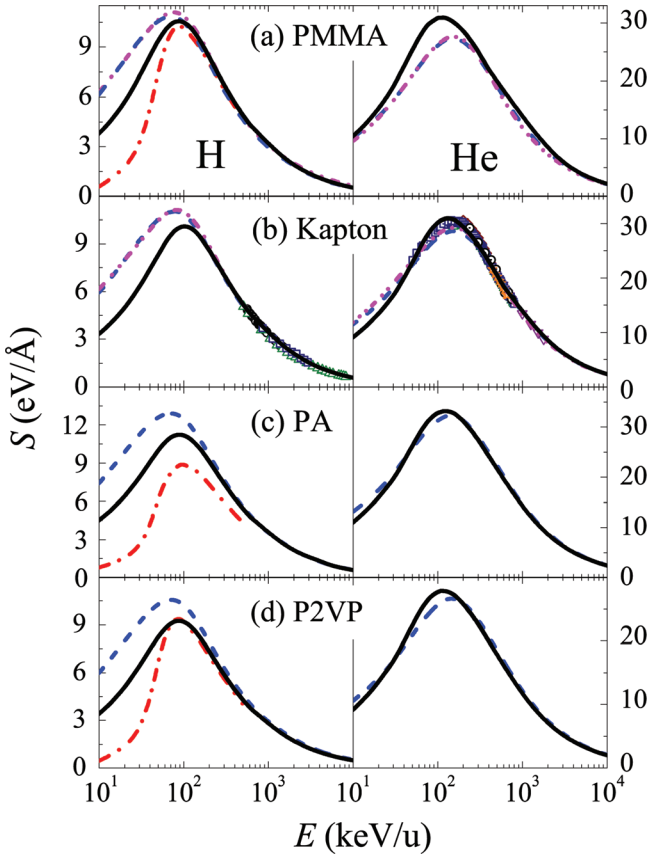

FIG. 4. (Color online) Stopping power of the four organic polymers, for proton and α-particle beams, as a function of incident kinetic energy: (a) PMMA, (b) Kapton, (c) PA, and (d) P2PV. Solid lines are the results obtained in this work with the MELF-GOS method. Symbols represent experimental data (only available for Kapton): Δ (Ref. 61), ⊙ (Ref. 62), ⊡ (Ref. 63), ∇ (Ref. 64) ◇ (Ref. 65) and ⋆ (Ref. 67). Other calculations are also shown: dashed lines from SRIM code (Ref. 68), dash-dot-dotted lines from ICRU (Ref. 50), and dash-dotted lines from Akkerman and Akkerman (Ref. 35).

charge state fractions ϕ_q from the CasP code,[32] which applies Bragg's rule to each elemental constituent of the compound target. Finally, the Brandt–Kitagawa theory[31] is used to compute the Fourier transform of the electronic density for each charge state, $f_q(k)$. In Fig. 4, experimental values for the stopping power of protons and α-particles for Kapton (which are the only available) and calculations by other models for the four polymers discussed are included for comparison.

As can be seen from the figure, the experimental values for protons[61–63] and α-particles[62–67] in Kapton are in excellent agreement with our calculations. It is more relevant in the case of helium ions because the experimental data (between 50 and 2000 keV/u) cover the range of the maximum stopping power, where the charge exchange and solid-state effects are stronger. Our calculations perfectly agree with the experimental data for protons too. In this case, the experimental values exist above 500 keV, where calculations are less sensitive to the method used to describe the target excitation spectrum.

In Fig. 4 we have depicted the results of other three semiempirical methods for calculating the stopping power: SRIM2008 (Ref. 68) (dashed lines), ICRU code PSTAR (Ref. 50) (dotted lines), and the approach of Akkerman and

Akkerman[35] (dash-dotted lines); SRIM and PSTAR give rather similar results in all the energy range for the polymers analyzed here. At high energies, all approaches also agree with the MELF-GOS method and with the experimental data. However, at low and intermediate energies, these codes predict different values of the stopping power. It is worth to note how differences appear at energies where aggregattion effects and charge-exchange mechanisms are stronger, a region where the stopping power obtained by the MELF-GOS method achieves an excellent agreement with the experimental data for α-particles in Kapton. Again, the reason for these differences lies in the different descriptions of the excitation spectrum of the target material, as it has been discussed in the previous section. SRIM (Ref. 68) and PSTAR (Ref. 50) make use of semiempirical formulas based on experimental data and theoretical trends, while Akkerman and Akkerman[35] use a linear combination of Drude functions to describe the optical ELF with a simple quadratic dispersion relation in k. Instead of this, the MELF-GOS method exploits the properties of the Mermin dielectric function for extrapolating the ELF($k=0,\omega$) in the entire (k-ω) plane, resulting in a more realistic description.

The interaction of ions with solids is a stochastic process and the stopping power S is a mean value the fluctuations of which are accounted for by the energy-loss straggling Ω^2 (see discussion in Sec. II A). In Fig. 5, we show the energy-loss straggling, Ω^2, for the polymers discussed in this work. As it can be seen, Ω^2 increases with the incident energy until reaching the Bohr straggling, given by $\Omega^2_{\text{Bohr}} = 4\pi Z_1^2 e^4 Z_2 \mathcal{N}$, when all the target electrons are excited. The corresponding values for protons and α-particles in PMMA, Kapton, PA, and P2PV are shown in Table VI.

Finally, it is worth to mention that Figs. 2, 3, and 4 show a quite similar behavior for the inelastic mean free path and

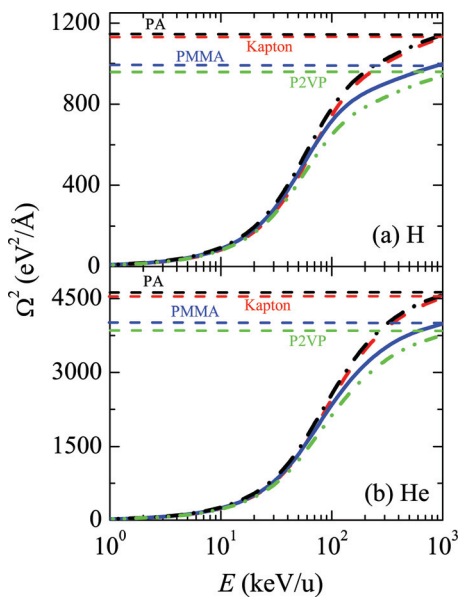

FIG. 5. (Color online) Energy-loss straggling calculated with the MELF-GOS method in this work for (a) proton and (b) α-particle beams interacting with: PMMA (solid line), Kapton (dashed line), PA (dash-dotted line), and P2VP (dash-dot-dot line). Horizontal lines represent the Bohr straggling for each polymer, as indicated by the respective labels.

TABLE VI. Bohr straggling for protons and α-particles for the four polymers studied in this work.

	Ω^2_{Bohr} (eV^2/Å)			
	PMMA	Kapton	PA	P2VP
H	1005	1139	1146	963
He	4018	4555	4586	3851

the stopping power of charged particles, respectively, of all polymers with a nearly universal behavior. This issue has been previously addressed by Tanuma *et al.*[30] regarding the inelastic mean free path of electrons. Similar arguments can be applied to the stopping power of electron and ion beams. Actually, almost all polymers have comparable chemical composition and density, as it can be seen in Table I, and their optical ELF are virtually identical (Fig. 1), so there is a very similar response of all the polymers to charged particles.

IV. SUMMARY AND CONCLUSIONS

In this work we report theoretical values of useful stopping magnitudes for studying the interaction of electron, proton, and α-particle beams in four commonly used organic polymers in a wide incident energy range. The energy range studied includes the region of the maximum stopping power and minimum inelastic mean free path, where the choice of the model used for predicting the stopping magnitudes is crucial because target aggregation and chemical bonding effects, as well as projectile charge-exchange mechanisms and quantum indistinguishability, are more significant.

We have calculated the inelastic mean free path, the stopping power, and the energy-loss straggling for electron, proton, and α-particle beams considering the aggregation and bonding effects through a realist description of the energy-loss function of the target material with the MELF-GOS method, which has the advantage of providing an automatic and analytical extension of the experimental optical ELF to $k \neq 0$ values by means of the properties of the Mermin dielectric functions and the GOS. Therefore a specific dispersion relation is not necessary as in other models. We also take into account the nature of the projectile: for ions, the charge-state fractions have been considered, and, for electrons, we include the exchange effect due to the quantum indistinguishability of the incident and target hitted electrons.

Our results are compared both with experimental data (when they are available) and with other semiempirical models. Although the measured data are scarce for electron beams, it is remarkable how our inelastic mean free path calculations perfectly agree with the experimental values for PMMA,[54] where better results than other methods have been achieved; the agreement with data for Kapton[55] and PA (Ref. 58) is reasonable. Even a better concordance is obtained when comparing the MELF-GOS method results with the experimental data existing for protons[61–63] and α-particles[62–67] interacting with Kapton: an excellent agreement has been achieved both at high energies (where the choice of the model is less important) and at low and

intermediate energies, where the differences between models are greater.

Also the parameterization with simple analytical formulas of the inelastic mean free path and the stopping power of electron beams will make easy its implementation in Monte Carlo simulation codes.

ACKNOWLEDGMENTS

Pablo de Vera acknowledges the Conselleria d'Educació de la Generalitat Valenciana for financial support under the VALi+d program. The authors also acknowledge financial support from the Spanish Ministerio de Ciencia e Innovación (Project FIS2010-17225).

[1]S. Gorelick, V. A. Guzenko, J. Vila-Comamala, and C. David, Nanotechnology. **21**, 295303 (2010).
[2]F. Yaghmaie, J. Fleck, A. Gusman, and R. Prohaska, Microelectron. Eng. **87**, 2629 (2010).
[3]H. G. Duan, E. Q. Xie, and L. Han, J. Appl. Phys. **103**, 046105 (2008).
[4]W. Hong, H. Woo, H. Choi, Y. Kim, and G. Kim, Appl. Surf. Sci. **169–170**, 428 (2001).
[5]F. S. Teixeira, M. C. Salvadori, M. Cattani, and I. G. Brown, J. Appl. Phys. **105**, 064313 (2009).
[6]D. Kirby, S. Green, H. Palmans, R. Hugtenburg, C. Wojnecki, and D. Parker, Phys. Med. Biol. **55**, 417 (2010).
[7]S. K. Mahapatra, S. D. Dhole, V. N. Bhoraskar, and G. G. Raju, J. Appl. Phys. **100**, 034913 (2006).
[8]J. Jagielski, A. Turos, D. Bielinski, A. M. Abdul-Kader, and A. Piatkowska, Nucl. Instrum. Methods B **261**, 690 (2007).
[9]W. M. Lau, Nucl. Instrum. Methods B **131**, 341 (1997).
[10]R. L. Clough, Nucl. Instrum. Methods B **185**, 8 (2001).
[11]P. Murugaraj, D. Mainwaring, N. A. Khelil, J. L. Peng, R. Siegele, and P. Sawant, Carbon. **48**, 4230 (2010).
[12]Y. Yun, C. Pearson, D. H. Cadd, R. L. Thompson, and M. C. Petty, Org. Electron. **10**, 1596 (2009).
[13]S. O. Kucheyev, T. E. Felter, M. Anthamatten, and J. E. Bradby, Appl. Phys. Lett. **85**, 733 (2004).
[14]H. Dong and T. Bell, Surf. Coat. Technol. **111**, 29 (1999).
[15]H. A. Bethe and J. Ashkin in *Experimental Nuclear Physics*, edited by E. Segre (Wiley, New York, 1953), Vol. I, pp. 166–201.
[16]W. H. Bragg and R. Kleeman, Phil. Mag. **10**, 318 (1905).
[17]D. I. Thwaites, Nucl. Instrum. Methods B **69**, 53 (1992).
[18]H. Paul and A. Schinner, Nucl. Instrum. Methods B **249**, 1 (2006).
[19]J. Lindhard, K. Dan. Vidensk. Selsk. Mat. Fys. Medd. **28**, (8) (1954).
[20]I. Abril, R. Garcia-Molina, C. D. Denton, F. J. Pérez-Pérez, and N. R. Arista, Phys. Rev. A **58**, 357 (1998).
[21]S. Heredia-Avalos, R. Garcia-Molina, J. M. Fernández-Varea, and I. Abril, Phys. Rev. A **72**, 052902 (2005).
[22]J. C. Moreno-Marín, I. Abril, and R. Garcia-Molina, Nucl. Instrum. Methods B **193**, 30 (2002).
[23]C. D. Denton, I. Abril, R. Garcia-Molina, J. C. Moreno-Marín, and S. Heredia-Avalos, Surf. Interf. Anal. **40**, 1481 (2008).
[24]S. Heredia-Avalos, J. C. Moreno-Marín, I. Abril, and R. Garcia-Molina, Nucl. Instrum. Methods B **230**, 118 (2005).
[25]J. C. Moreno-Marín, I. Abril, S. Heredia-Avalos, and R. Garcia-Molina, Nucl. Instrum. Methods B **249**, 29 (2006).
[26]M. Behar, R. C. Fadanelli, I. Abril, R. Garcia-Molina, C. D. Denton, L. C. C. M. Nagamine, and N. R. Arista, Phys. Rev. A **80**, 062901 (2009).
[27]J. Brandrup, E. H. Immergut, E. A. Grulke, A. Abe, and D. R. Bloch, *Polymer Handbook*, 4th ed. (Wiley, New York, 2003)
[28]DuPont webpage: http://www2.dupont.com/DuPontome/enS/index.html.
[29]V. N. Salimgareeva, N. S. Sannikova, S. V. Kolesov, and Z. Kh. Kuvatov, Russ. J. Appl. Chem. **74**, 478 (2001).
[30]S. Tanuma, C. J. Powell, and D. R. Penn, Surf. Interf. Anal. **21**, 165 (1993).
[31]W. Brandt and M. Kitagawa, Phys. Rev. B **25**, 5631 (1982).
[32]G. Schiwietz and P. L. Grande, Nucl. Instrum. Methods B **175**, 125 (2001). The CasP code can be downloaded from: http://www.helmholtz-berlin.de/people/gregor-schiwietz/caspn.html.
[33]N. D. Mermin, Phys. Rev. B **1**, 2362 (1970).
[34]R. H. Ritchie and A. Howie, Phil. Mag. **36**, 463 (1977).
[35]A. Akkerman, A. Breskin, R. Chechik, and Y. Lifshitz, Rad. Phys. Chem. **61**, 333 (2001).
[36]Z. Tan, Y. Xia, M. Zhao, and X. Liu, Nucl. Instrum. Methods B **248**, 1 (2006).
[37]A. Akkerman and E. Akkerman, J. Appl. Phys. **86**, 5809 (1999).
[38]D. J. Planes, R. Garcia-Molina, I. Abril, and N. R. Arista, J. Electron. Spectrosc. Relat. Phenom. **82**, 23 (1996).
[39]R. Garcia-Molina, I. Abril, C. D. Denton, S. Heredia-Avalos, I. Kyriakou, and D. Emfietzoglou, Nucl. Instrum. Methods B **267**, 2647 (2009).
[40]R. F. Egerton, *Electron Energy-Loss Spectroscopy in the Electron Microscope* (Plenum, New York, 1989).
[41]J. J. Ritsko, L. J. Brillson, R. W. Bigelow, and T. J. Fabish, J. Chem. Phys. **69**, 3931 (1978).
[42]E. T. Arakawa, M. W. Williams, J. C. Ashley, and L. R. Painter, J. Appl. Phys. **52**, 3579 (1981).
[43]J. J. Ritsko, Phys. Rev. B **26**, 2192 (1982).
[44]J. J. Ritsko and R. W. Bigelow, J. Chem. Phys. **69**, 4162 (1978).
[45]G. Mondio, F. Neri, S. Patane, A. Arena, G. Marletta, and F. Iacona, Thin Solid Films **207**, 313 (1992).
[46]B. L. Henke, E. M. Gullikson, and J. C. Davis, At. Data Nucl. Data Tables **54**, 181 (1993). The ASCII files for the f_1 and f_2 scattering factors of the different elements can be downloaded from http://xray.uu.se/hypertext/henke.html.
[47]G. P. Williams, in *X-ray Data Booklet*, edited by A. C. Thompson (Lawrence Berkeley National Laboratory, University of California, Berkley, California, 2009), Section 1-1. The binding energies of the elements can be downladed from http://xdb.lbl.gov/Section1/Sec-1.html.
[48]M. Inokuti, Rev. Mod. Phys. **43**, 297 (1971).
[49]ICRU37, Stopping Powers for Electrons and Positrons (ICRU Report Vol. 37, International Commission on Radiation Units and Measurements, Bethesda, MD, 1984).
[50]ICRU49, Stopping Powers and Ranges for Protons and Alpha Particles (ICRU Report Vol. 49, International Commission on Radiation Units and Measurements, Bethesda, MD, 1992).
[51]Z. Tan, Y. Xia, M. Zhao, X. Liu, F. Li, B. Huang, and Y. Ji, Nucl. Instrum. Methods B **222**, 27 (2004).
[52]L. E. Porter, Int. J. Quantam. Chem. **75**, 943 (1999).
[53]J. M. Fernández-Varea, R. Mayol, D. Liljequist, and F. Salvat, J. Phys.: Condens. Matter **5**, 3593 (1993).
[54]R. F. Roberts, D. L. Allara, C. A. Pryde, D. N. E. Buchanan, and N. D. Hobbins, Surf. Interf. Anal. **2**, 5 (1980).
[55]P. Cadman, G. Gossedge, and J. D. Scott, J. Electron. Spectrosc. Relat. Phenom. **13**, 1 (1978).
[56]B. Lesiak, A. Kosinski, M. Krawczyk, L. Zommer, A. Jablonski, J. Zemek, P. Jiricek, L. Kövér, J. Tóth, D. Varga, and I. Cserny, Appl. Surf. Sci. **144–145**, 168 (1999).
[57]B. Lesiak, A. Kosinski, M. Krawczyk, L. Zommer, A. Jablonski, L. Kövér, J. Tóth, D. Varga, I. Cserny, J. Zemek, and P. Jiricek, Polish J. Chem. **74**, 847 (2000).
[58]G. Gergely, M. Menyhard, A. Sulyok, S. Gurban, B. Lesiak, A. Jablonski, A. Kosinski, J. Tóth, and D. Varga, Cent. Eur. J. Phys. **5**, 188 (2007).
[59]K. Kumagai, S. Tanuma and C. J. Powell, Nucl. Instrum. Methods B **267**, 167 (2009).
[60]P. Sigmund, *Particle Penetration and Radiation Effects* (Springer-Verlag, Berlin, 2002).
[61]J. Räisänen and E. Rauhala, Phys. Rev. B **35**, 1426 (1987).
[62]W. E. Wallace, J. B. Rothman, and R. J. Composto, J. Appl. Phys. **75**, 2312 (1994).
[63]A. J. M. Plompen, F. Munnik, J. Räisänen, and U. Wätjen, J. Appl. Phys. **80**, 3147 (1996).
[64]Á. Z. Kiss, E. Somorjai, J. Räisänen, and E. Rauhala, Nucl. Instrum. Methods B **39**, 15 (1989).
[65]K. Takahiro, F. Nishiyama, T. Yamasaki, Y. Osaka, and S. Yamaguchi, Nucl. Instrum. Methods B **52**, 117 (1990).
[66]J. Räisänen, U. Wätjen, A. J. M. Plompen, and F. Munnik, Nucl. Instrum. Methods B **118**, 1 (1996).
[67]M. Chekirine and H. Ammi, Radiat. Measur. **30**, 131 (1999).
[68]J. F. Ziegler, J. P. Biersack, and M. D. Ziegler, *SRIM. The Stopping and Range of Ions in Matter* (SRIM Co., Maryland, 2008).